Developing and testing a computer vision method to quantify 3D movements of bottom-set gillnets on the seabed

Savina, Esther; Krag, Ludvig Ahm; Madsen, Niels

Developing and testing a computer vision method to quantify 3D movements of bottom-set gillnets on the seabed

Esther Savina[a], Ludvig Ahm Krag[a], Niels Madsen[a*]

[a] Technical University of Denmark, National Institute of Aquatic Resources, Willemoesvej 2, 9850 Hirtshals, Denmark

[*] Section of Biology and Environmental Science, Department of Chemistry and Bioscience, Aalborg University, Fredrik Bajers Vej 7, 9220 Aalborg, Denmark

CORRESPONDING AUTHOR

Esther Savina, esav@aqua.dtu.dk, +45 35 88 32 02

Technical University of Denmark, National Institute of Aquatic Resources, Willemoesvej 2, 9850 Hirtshals, Denmark

KEYWORDS:

Coastal waters; Environmental impact; Fishing gear; Gillnet; Habitat; Stereo vision

HIGHLIGHTS

- A stereo imaging method was adapted to quantify in situ fishing gear habitat effect.
- The movement of the leadline of light and heavy bottom gillnets on sand was assessed.
- The direct mechanical damage to the seabed (penetration) of gillnets was minimal.
- The sweeping movements were higher than estimated by experts, up to 2 m.
- Light nets were moving significantly more than heavy ones.

ABSTRACT

1 Gillnets are one of the most widely used fishing gears, but there is limited knowledge about
2 their habitat effects, partly due to the lack of methodology to quantify such effects. A stereo
3 imaging method was identified and adapted to quantify the dynamic behavior of gillnets in-
4 situ. Two cameras took synchronized images of the gear from slightly different perspectives,
5 allowing to estimate the distance from the observation unit to the gear such as in the human 3D
6 vision. The sweeping motion on the seabed and the penetration into the sediment of the leadline
7 of light and heavy commercial bottom gillnets deployed in sandy habitats in the Danish coastal
8 plaice fishery were assessed. The direct physical disruption of the seabed was minimal as the
9 leadline was not penetrating into the seabed. Direct damage to the benthos could however
10 originate from the sweeping movements of the nets, which were found to be higher than usually
11 estimated by experts, up to about 2 m. The sweeping movements were for the most part in the
12 order of magnitude of 10 cm, and resulted in a total swept area per fishing operation lower than
13 any of the hourly swept area estimated for active fishing gears. Whereas the general perception
14 is that heavy gears are more destructive to the habitat, light nets were moving significantly
15 more than heavy ones. The established methodology could be further applied to assess gear
16 dynamic behavior in-situ of other static gears.

17   **1. Introduction**

18   Ecosystem effects of fisheries and in particular habitat damage is of high interest in an

19   Ecosystem Approach to Fisheries as some fishing gears can remove or damage habitat forming

20   structures, potentially reducing the complexity, diversity and productivity of benthic

21   environments (Jennings and Kaiser, 1998; Kaiser *et al.*, 2000; Kaiser *et al.*, 2002; Hermsen *et*

22   *al.*, 2003; Grabowski *et al.*, 2014). The Marine Strategy Framework Directive defines seabed

23   integrity as one of the descriptors required by the European Union member states to ensure

24   Good Ecological Status (E.C., 2008). Methods are being developed for assessing the

25   responsiveness of different seabed habitats to fishing activities, resulting in habitat sensitivity

26   maps, which can be used in marine spatial planning (Eno *et al.*, 2013). Eco-labelling initiatives

27   have started to take gear impacts on habitats into account in their assessments (Olson *et al.*,

28   2014). In this context, providing documentation for the habitat effect of fishing gears is of prime

29   importance, especially for small-scale fisheries where maintaining profitability may be

30   challenging and where there are benefits to keeping fishing in traditional fishing grounds,

31   including sensitive areas, or where higher prices could be obtained from eco-labelling.

32   Gillnets stand as the fourth most important general gear type (out of 8) contributing to the

33   global marine catches (in weight, based on data from 1950 to 2001, Watson *et al.*, 2006). About

34   40% of the European fishing vessels belong to the small-scale bottom-set gillnets fleet (by

35   number, as of December 2016), with 33 644 active vessels under 12m with set gillnets (GNS) as

36   main gear, and up to 80% in Denmark for example (by number, with 1838 active vessels under

37   12m with GNS as main gear as of December 2016) (E.C., 2016). It is generally assumed that

38   habitat impacts of fixed gears are lower than those of mobile gears (Suuronen *et al.*, 2012;

39   Grabowski *et al.*, 2014). However, these conclusions are based on few experimental studies. For

40   example, there were only five studies regarding fixed gears, i.e., longlines, traps and gillnets, out

41   of 97 used for the latest assessment in New England, US (Grabowski *et al.*, 2014). Taking a

42   closer look at bottom gillnets, the lack of studies regarding habitat impact might be attributed to

43   the general assumption of negligible effects (Uhlmann and Broadhurst, 2013). However, after in

44   situ observation at two rocky reefs, Shester and Micheli (2011) identified set gillnets as a

45   priority conservation concern due to their potential to damage habitat-forming species. In the

46   Welsh part of the Irish Sea, Eno *et al.* (2013) assessed nets sensitivity as high to medium for

47   high to low fishing intensities in 8 habitats out of 31, mostly rock with associated branching

48   species such as kelp, seaweeds or maerl beds. There is no direct evidence of potential effect for

49   many of the current habitat-gear combinations, and the degree to which fixed gears drift on the

50   bottom has to be quantified for the different bottom types (Eno *et al.*, 2013; Grabowski *et al.*,

51   2014).

52   There is limited knowledge about the habitat effects of bottom gillnets partly due to historical

53   focus on active gears, but also because data collection and analysis calls for the development of

54   appropriate innovative assessment methodologies. Several optical or acoustic techniques have

55   been developed as complementary tools to assess the impact of mobile gears on the seabed

56   (Smith *et al.*, 2003; Humborstad *et al.*, 2004; O'Neill *et al.*, 2009; Lucchetti and Sala, 2012;

57   Depestele *et al.*, 2016). However, not all techniques provide a spatial resolution fine enough to

58   assess bottom gillnets. Others are restrictive in sampling duration. Eventually, not all techniques

59   can easily and safely be operated around bottom gillnets, prone to entanglement. Video offers

60   more precision and less bias than direct visual observation, as it is possible to view each

61   recording repeatedly or at lower speed (Neuswanger *et al.*, 2016). Nevertheless, the value of a

62   video recording as informative data also depends on the ability to extract relevant measurements

63 (Struthers *et al.*, 2015; Neuswanger *et al.*, 2016). Waterproof action cameras are now commonly

64 available tools to deliver cost efficient high-definition underwater video recordings (Struthers *et*

65 *al.*, 2015) using simple deployment platforms.

66   In bottom-set gillnets, the gear components in contact with the seabed are the leadline, the

67 anchors and the bridle lines (connecting the anchors to the netting). Gillnets may be dragged on

68 the seabed and become tangled in bottom features as the gear moves with the water flow while

69 fully deployed on the seabed. Gillnets may also be snagged on benthic structures or organisms

70 during retrieval of the gear (Shester and Micheli, 2011). The gear characteristics and rigging

71 specifications play a key role in the net behavior, and therefore its potential seabed effects. The

72 net is spread vertically by the buoyancy of floats on the headline and weight in the leadline

73 (Takagi *et al.*, 2007; He and Pol, 2010). The gear is usually moored at both ends with weights or

74 anchors, which can cause vertical and horizontal deformation of the netting (Shimizu *et al.*,

75 2007; He and Pol, 2010). Water flow pushes the netting to incline and bulge out of the vertical

76 plane (Stewart, 1988; Takagi *et al.*, 2007). Shimizu *et al.* (2007) calculated that the leadline

77 would slide across the sea bottom if the force acting on the leadline is larger than the coefficient

78 of static friction, but sliding motions of bottom gill nets during fishing have not been directly

79 observed in any study to our knowledge.

80   The aim of the study was to identify, adapt, test and use a suitable methodology for assessing

81 the dynamic behavior of the leadline of bottom gillnets, i.e., the sweeping motion on the seabed

82 and the penetration into the sediment. An in-situ pilot experiment using stereo imaging was

83 carried out in the Danish gillnet coastal plaice fishery.

84 **2. Material and methods**

85 **Stereo imaging: general principle and quantitative measurements with VidSync**

86   Stereo imaging consists of two cameras taking synchronized images of a scene from slightly

87 different perspectives, or vantage points, which then allow to estimate the distance to an object

88 such as in the human 3D vision. If an object is uniquely identified in both images and if the

89 translation and rotation of one camera relative to the second is known, it is then possible to

90 estimate the location of the object in 3D space (Schmidt and Rzhanov, 2012).

91   The free open-source Mac application VidSync (www.vidsync.org) was developed based on

92 the OpenCV library computer vision algorithms by Neuswanger *et al.* (2016) to process stereo

93 video recordings. The mathematical calculations of 3D measurements and their application in

94 VidSync are detailed by Neuswanger *et al.* (2016).

95   Before the proper calculation of the 3D coordinates of a point, one has to correct for lens

96 distortion and establish the perspective of each camera. Lens distortion is induced by the fisheye

97 lens of the camera, meant to widen its angle of view, but particularly pronounced when the

98 camera records underwater through housing and prone to bias calculations. Correction factors,

99 or distortion parameters, can be found by locating nodes on a chessboard pattern or calibration

100 frame and arranging them into straight lines. The same chessboard pattern can be used to

101 calculate the projection matrices for each camera by matching the known physical 2D node

102 coordinates on each face of the calibration frame with screen coordinates, which are recorded in

103 VidSync by clicking on the centre of each node on the video recordings.

104   The 3D coordinates of a point are calculated in VidSync by iterative triangulation, aiming at

105 establishing two lines-of-sight that approximately intersect at the point of interest, which is

106 undertaken by clicking on the different points of the leadline, on each video recording. The

107   calibration frame is the only source of information on the scaling of distances from which

108   VidSync reconstructs a 3D space from the 2D video recordings.

109   **Pilot experiment: location of the sea trials, net type and gear specifications**

110   The pilot experiment took place in ICES area IIIa (Kattegat) off the coast of Northern

111   Denmark aboard a small research vessel (5 m) on September 10th 2015. Because of its

112   importance regarding Danish traditional commercial fishing grounds, and as the probability that

113   the leadline would slide across the sea bottom is higher for smooth surfaces than for rough

114   surfaces (Shimizu *et al.*, 2007), the experiment took place on sandy bottom. Nets were deployed

115   in shallow waters, i.e., 1.5 to 3 m depth, to operate the observation units as best as possible in

116   relation to the deployed gillnets in the relatively turbid waters. Our experimental conditions

117   were at the lower depth range of commercial practices, but many coastal vessels participating in

118   the gillnet plaice fishery, usually fish between 2 and 8 m in the summer and autumn. All

119   observations were made away from the surf zone in calm weather to limit the influence of

120   waves.

121   Two different types of commercial bottom gillnets, light and heavy, were used to give a

122   gradient of commercial conditions. All nets were commercial plaice gillnets, and heavy and light

123   nets differed only in the specifications of the head- and leadlines (Table 1). The headline was

124   different for the two gear types as it influences the inclination of the net and has commonly more

125   buoyancy for heavier nets in commercial conditions. It is commercial practice to work with such

126   a net height when targeting plaice (1.1 m). Mesh size was selected according to the fish target at

127   the chosen trial location, i.e., plaice on sandy habitat. Both net types were made by Daconet

128   (www.daconet.dk) with the same manufacturing process.

129   **Pilot experiment: stereo recording units and their calibration**

130   Each observation unit was composed of a simple metallic frame made of 1 cm diameter steel

131   sticks (Fig. 1). Each metallic frame was ballasted with concrete poured in 7.5 cm diameter and

132   12.5 cm long polyvinyl chloride (PVC) tubes at each foot. The use of a light frame ensured a

133   surface as small as possible for limiting drag, whereas the heavy feet guaranteed that the frame

134   would remain in position when lowered on the seabed. Two cameras in their waterproof housing

135   were mounted on the frame at a distance of 65 cm from each other and protected by netting (Fig.

136   1). The use of netting aimed at preventing entanglement of the netting of the gillnet into the

137   frame when in contact. Cameras were GoPro Hero 3 and 3+ cameras, each pair of a recording

138   unit having identical settings (type of camera and video mode). For all fleets, the video

139   resolution was set to 1080p SuperView, i.e., the sides of the video were stretched out for greater

140   viewing, the frame per second was set to 30, and the field of view was set to Ultra Wide. Initial

141   testing of the set-up with resolution set to 4K and frame per second set to 12 resulted in

142   measurement errors exceeding 25%.

143   A 3D calibration frame of 80 x 51 x 31 cm with a 9-by-15 node pattern in the front face and

144   an 8-by-5 node pattern in the back face was used (Fig. 2). The front face was made of perspex

145   acrylic glass (PMMA) (http://vink.dk/), which can refract light when looking at the back frame

146   and slightly change the apparent position of the nodes (Neuswanger *et al.*, 2016). A correction

147   was applied to compensate for light refraction by the front frame based on the thickness of the

148   material (35mm), the refractive index of the material (PMMA, 1.491), and the refractive index

149   of the medium (salt water, 1.342) (Neuswanger *et al.*, 2016).

150   Each observation unit, consisting of two cameras mounted on a metallic frame was submerged

151   in water and calibrated at the Nordsøen Oceanarium (http://nordsoenoceanarium.dk/).

Pilot experiment: experimental set-up and measurement of water flow speed

152

153   Three individual net panels were attached at the floatlines to form a fleet, similar to

154   commercial practice (Fig. 3a). All fleets were set in a straight line parallel to the coast and the

155   predominant current direction. Fleets were anchored at both ends with four kg anchors using six

156   metres bridle lines following commercial practices. As the motion at a specific section of the net

157   depends on its relative position (Shimizu *et al.*, 2004), each stereo recording unit was positioned

158   on the seabed facing the middle length of the fleet, i.e., the part of the net the most likely to slide

159   assuming that the nets are set in a straight line, at about 1 to 2 m from the net (Fig. 3b). Three

160   fleets were soaked at the same time for two to three hours during the day. Fleets soaked together

161   formed a run. Data was collected while the gear was fully deployed on the seabed.

162   Nets were marked with different red tape patterns on the leadline to ensure that these marks

163   would easily be uniquely identified on the video recordings (Fig. 3 and 4). A high resolution

164   clock (B. Lundgren, pers. comm.) was recorded at the beginning of every recording, providing a

165   distinctive feature to synchronize the video recordings from the left and right cameras to the

166   nearest video frame.

167   The water speed was recorded using two sets of a GPS device (GP-102,

168   www.canmore.com.tw) attached to a buoy and left drifting during data collection (Fig. 5). A

169   holed PVC tube with attached lead hanging from the buoy was used to make sure that the

170   measurement gave the current speed in the water column and not at the surface (wind drift). Use

171   of the flow speed average from the bottom up to the net height could lead to more precise

172   calculation by incorporating vertical difference in flow speed caused by the bottom boundary

173   layer, but it is commonly accepted to use the current speed measured at the median net height in

174   the mid-point location between the nets (Matuda and Sannomiya, 1977a, b; Matuda and

175   Sannomiya, 1978; Matuda, 1988; Shimizu *et al.*, 2007).

176   Hourly instantaneous horizontal seawater velocities (2D) at 1m depth were also extracted

177   from the Forecasting Ocean Assimilation Model 7 km Atlantic Margin model (FOAM AMM7)

178   (EU Copernicus, 2017). The 7 km resolution of the model restricts its utility in the coastal zone

179   where strong sub-grid scale variability in shallow water bathymetry affects the wave field, and

180   modelled data was therefore used as an overall indication of water flow speed in the area, but

181   not for instantaneous measurement at each net position.

182   **Pilot experiment: data analysis**

183   The position of the calibration frame defined the 3D coordinate system, i.e., the origin (0, 0,

184   0) was the bottom left point on the front face of the calibration frame, the front and back faces

185   were found in the *x-z* plane, with the front face in the plane *y*=0 and the back face in the plane

186   *y*=distance between both faces (Fig. 2). Thus, the net movements in the X dimension were

187   positive when the net moved rightward or negative leftward (Fig. 4). The movements in the Y

188   dimension were positive when the net moved backward or negative forward. As the observation

189   units were facing the coast during deployment, the movements in the Y dimension were positive

190   when the net moved towards the coast and negative towards the open sea. The movements in the

191   X and Y dimensions represent the sweeping motion of the net. The movements in the Z

192   dimension were positive when the net moved upward, i.e., lifting off the seabed, or negative

193   downward, i.e., dropping on the seabed. The movements in the Z dimension represent the seabed

194   penetration.

195   We checked for data entry mistakes or calibration problems by examining diagnostic error

196   measures provided for each 3D point by Vidsync (Neuswanger *et al.*, 2016). To quantify actual

197   errors in 3D measurements, the calculated (VidSync) and measured (measuring tape) distances

198   between two nodes as well as between the two faces of the calibration frame were compared in a

199   first control test, and the calculated and measured distances between two coloured threads on the

200   leadline of both light and heavy gillnets were compared in a second control test. The first point

201   calculated was set as a reference starting point with a given position of zero in the three

202   dimensions, and the position value of this reference point was subtracted from the position

203   values of the following points. The dynamic behavior of the leadline was analysed using a

204   simple motion metrics in the three spatial dimensions, i.e., the maximum distance covered by the

205   leadline in each dimension, calculated as the difference between the maximum and the minimum

206   position values of each mark.

207   Significant differences between light and heavy net configurations were tested for as follows.

208   Data exploration was applied following Zuur *et al.* (2010). The effect of net configuration (light

209   or heavy), run (I or II) and dimension (X, Y or Z) on the maximum movement of the leadline

210   was initially modelled as a linear regression model containing sensible interactions based on

211   experimental knowledge and data exploration as in model (1). A log-transformation was applied

212   on the response variable as a solution to heterogeneity of variance. As the video recording

213   duration varied between marks (Table 2), duration was used as an offset. The linear regression

214   model is given by:

215     $\log(Y_i) = \beta\,(\text{Dimension}_i,\, \text{Net}_i,\, \text{Run}_i) + 1*\log(\text{Duration}_i) + \varepsilon_i$ with $\varepsilon_i \sim N(0,\, \sigma_i^2)$ (1)

216   where Y_i is the maximum movement of the ith mark, β is the population slope and ε_i is the

217   residual normally distributed with expectation 0 and variance σ_i^2.

218   Model selection was applied to model (0) by dropping individual explanatory variables one by

219   one based on hypothesis testing (F-statistic), and resulted in the preferred model (2):

220    $\log(Y_i) = \beta\ (\text{Dimension}_i) + \gamma\ (\text{Net}_i, \text{Run}_i) + 1*\log(\text{Duration}_i) + \varepsilon_i$ with $\varepsilon_i \sim N(0, \sigma_i^2)$ (2)

221   All parameters were tested significant at p-value <0.001. The four assumptions that allow the

222   sample data to be used to estimate the population data are: normality, homogeneity,

223   independence and fixed explanatory variable (i.e., measurement error in the explanatory variable

224   is small compared to the noise in the response variable). The chosen model (2) was validated by

225   visual inspection of the residuals.

226   The video recordings were processed with VidSync version 1.66 (www.vidsync.org). All

227   other analyses were performed by the open-source software R 3.2.3 (R Core Team, 2016).

228   **3. Results**

229   **Data collected and error measures**

230   Video recordings from five fleets were clear and long enough for analysis, i.e., three fleets for

231   run I and two fleets for run II (Table 2). Nets were deployed at 3 and 1.5-2 m depth,

232   respectively, for runs I and II. All video recordings were collected in good weather and sea

233   conditions. Modelled hourly water velocities were (average ± standard deviation) 0.049 ±0.003

234   and 0.031 ±0.027 m.s-1, respectively, for runs I and run II, which was in agreement with

235   measured water velocities of 0.028 ±0.025 m.s-1 for run II. A total of eight marks could be

236   uniquely identified on the leadline, i.e., one mark for fleet Ia, Ib, IIa, two marks for fleet Ic and

237   three marks for fleet IIb (Table 2). Total video recordings duration per mark ranged from 13 to

238   138 minutes, with an average of (mean ±standard deviation) 73 ±84 min for light nets and 109

239   ±41 min for heavy nets (Table 2). An extract of one of the recordings is given as an example

240   (supplementary material).

241   Diagnostic error measures provided for each 3D point by Vidsync did not show any data

242   entry mistake or calibration problem.

243   Distortion corrections reduced the distortion error, i.e., the distance between the input screen

244   points and the reprojected screen points, by (mean ±standard deviation) 54 ±12% for all cameras

245   in all recording units. The remaining distortion per point was 0.94 ±0.21 pixels on average for

246   all cameras in all recording units. There was a slight increase in absolute error for calculations

247   near the edge or centre of the screen for some of the video recordings.

248   In the first control test, the calculated (Vidsync) and measured (measuring tape) distances

249   between two nodes as well as between the two faces of the calibration frame were compared.

250   The Vidsync calculated distances were quite close to the measurements of the real distances,

251   with on average all measurement errors smaller than 10% (Fig. 6a).

252   In a second control test, the calculated (Vidsync) and measured (measuring tape) distances

253   between two coloured threads on the leadline of three light and four heavy gillnets were

254   compared. The Vidsync calculated distances were quite close to the measurements of the real

255   distances, with on average all measurement errors smaller than 25% (Fig. 6b). However, overall,

256   measurement errors for heavy nets in run I were up to around 150%, underestimating the

257   calculated distances compared to the measured ones.

258   Based on in-situ stereo vision measurements, the presented methodology can quantify the

259   dynamic behavior of the leadline of commercial bottom gillnets gillnet.

260   **Dynamic behaviour of the leadline and maximum distance covered by the leadline**

261   Marks were either stationary, e.g., mark 1 in the Y dimension, moved regularly continuous,

262   e.g., mark 1 in the X dimension, or moved with a sudden step, e.g., mark 6 in the X and Y

263   dimension (Fig. 7). Overall, marks on the same net moved similarly, e.g., marks 3 to 5 on fleet

264   Ic, even though local disparities were found, e.g., marks 7 and 8 on fleet IIb (Fig. 7). When

265   moving, all marks moved in a single direction in all dimensions, e.g., to the right only for mark

266   1 or to the left only for mark 6 (Fig. 7). However, not all fleets moved in the same direction, e.g.,

267   not all moved leftwards or towards the coast (Fig. 7).

268   The leadline was moving but not penetrating into the seabed as seen from the recorded

269   images, downward movements as calculated values in the Z dimension being most likely due to

270   slight disparities in the seabed features. The leadline was apparent in most of the footages,

271   except in rare occasions in which about five cm in length were not visible. The sea bottom was

272   slightly bumpy and it was not possible to see if the leadline was covered by sand or only behind

273   a bump in these few occasions.

274   The maximum distance covered by each mark on the leadline ranged from 0.14 to 1.10m,

275   0.06 to 2.01m and 0.02 to 0.26m in the X, Y and Z dimensions, respectively, with an average of

276   (mean ±standard deviation) 0.96 (±0.20) for light and 0.31 (±0.15) m for heavy nets, 1.5 (±0.67)

277   for light and 0.38 (±0.25) m for heavy nets, and 0.14 (±0.17) for light and 0.06 (±0.03) m for

278   heavy nets, in the X, Y and Z dimensions, respectively (Table 2). The maximum swept area

279   covered by the movements of each observed mark (X and Y dimensions) ranged from 0.02 to

280   1.65m2, with an average of 1.41 (±0.34) and 0.13 (±0.15) m2 for light and heavy nets,

281   respectively (Table 2). The leadline movements in the three dimensions were found to be

282   significantly different, with larger maximum movements in the Y dimension (Table 3).

283   Whatever the net type, the leadline moved 1.14 (0.49-2.65) times more in the Y dimension

284   (backward-forward) than in the X dimension (rightward-leftward), and 7.30 (3.15-16.89) times

285   more in the Y than in the Z dimension (upward-downward) (Fig. 8).

286   **Differences between net types and runs**

287   The leadline movements were significantly different for the two tested net configurations: for

288   both runs, light nets were moving more than heavy nets (Table 3). Whatever the dimension, light

289   nets moved 32.53 (95% confidence limits: 11.01-96.09) times more than heavy nets in run I, and

290   1.41 (0.43-4.61) in run II (Fig. 8). A significant interacting effect of runs (Table 3) was found,

291   with both light and heavy nets moving more in run I than run II. Light nets moved 26.79 (6.81-

292   105.47) times more in run I than in run II, and heavy nets moved 1.16 (0.50-2.68) times more in

293   run I than in run II. This is in line with higher water velocities in run I compared to run II.

294   **4. Discussion**

295   **Stereo-imaging for quantifying gear dynamic behavior in-situ**

296   The dynamic behavior of the leadline of commercial bottom gillnets could be quantified in

297   details using the presented methodology based on measurements of in-situ stereo vision

298   recordings. The methodology quantify both the seabed penetration and sweeping motion of the

299   leadline. This methodology can be further applied to assess habitat effect of other gear types,

300   especially other static gears such as creels and pots, or more generally further assess gear

301   dynamic behavior in-situ. Indeed, as net geometry affects the gear selectivity, an improved

302   understanding of the gear dynamic behavior would provide a better insight into the capture

303   process (Shimizu *et al.*, 2004; Herrmann *et al.*, 2009).

304   The stereo-imaging experimental set-up, i.e., the choice of camera separation and the

305   dimensions and position of the calibration frame, was configured to measure relatively small

306   objects close to the cameras. Accuracy and precision decreased as distance from the cameras

307   increased. The nets were not expected to move in such an order of magnitude, but a larger

308   chessboard, i.e., large enough to fill the screen, could have helped limit our measurement errors.

309   The fish eye effect could be reduced by limiting the field of view (instead of choosing ultra wide

310   setting).

311   A variety of challenges were faced when deploying the observation units near the nets at sea,

312   among which water turbidity, also noticed as a limitation for optical methods by Lucchetti and

313   Sala (2012) and Struthers *et al.* (2015). The video recordings could also appear blurry due to the

314   scattering effects of particles in the water column, and images could be exposed differently from

315   the two cameras due to irregular lightning and displacement between the cameras (Schmidt and

316   Rzhanov, 2012). These optical limitations reduced the number of recorded images that could be

317   processed. A camera that only captures light reflected from objects further away than a certain

318   distance could be used to remove the effects of scattered light and therefore solve the issue of

319   water turbidity (under development, L.A. Krag, pers. comm.).

320   Calibration and distortion corrections obtained in a tank were used for processing the in-situ

321   video recordings. The same camera specifications, i.e., camera settings and relative orientation,

322   for each recording unit, were used but any optical adjustment such as removing a camera from

323   its underwater housing to change a battery or a change of the angle between the cameras during

324   transportation/aboard the vessel may have affected the parameters and therefore the results. The

325   control tests did not show major issues, and one can therefore rely on the order of magnitude of

326 the results. But, the cameras should remain fixed throughout the experiment in a later use of the

327 stereo-imaging method.

328 **Pilot estimation of gillnets 3D dynamic behaviour and their seabed effects**

329 The leadline of bottom gillnets, fully deployed on the bottom, could sweep the seabed in

330 sandy habitats up to about 2 m, for the most part in the order of magnitude of 10 cm.

331 Movements were either continuous or in a sudden step, which was different from the periodical

332 displacement observed by Shimizu *et al.* (2004). This could be due to a different initial net shape

333 and spread of the leadline for each fleet when reaching the sea bottom (Shimizu *et al.*, 2007), or

334 local water flow disparities. The in-situ measurements of the leadline showed that movements

335 were the smallest in the Z dimension, less than a few centimeters. The leadline was moving but

336 not penetrating into the seabed as seen from the recorded images, downward movements as

337 calculated values in the Z dimension being most likely due to slight disparities in the seabed

338 features.

339 In terms of seabed disturbance, this means that the physical disruption of the seabed

340 (penetration) of gillnets is minimal compared to the sweeping of the gear, whereas seabed

341 penetration was observed as partly responsible for habitat physical impact in active fishing gears

342 (Eigaard *et al.*, 2016; Depestele *et al.*, 2016). The potential direct damage to the benthos would

343 therefore originate from the sweeping movements of the gillnets, as the leadline and netting can

344 snag and entangle available entities. The sweeping movements of plaice gillnets in the Danish

345 fishery were found to be higher than usually estimated by experts, but cannot be compared to

346 other in-situ measurements as these are the first quantitative measurements to our knowledge. A

347 maximum of 30 kms of nets are soaked in a typical bottom-set gillnets fishing operation

348 (Montgomerie, 2015). The swept area can roughly be estimated to about 0.04 km^2 for light nets

349   and 0.01 km^2 for heavy nets (based on a rectangle area calculation using the average measured

350   range per mark in the Y dimension as presented above, i.e., 1.5 for light and 0.38 m for heavy

351   nets). This is lower than any of the hourly swept area estimated for active fishing gears by

352   Eigaard *et al.* (2016), ranging from 0.05 km^2 for beam trawl to 1.5 km^2 for Scottish seining

353   surface impact. However, the swept area of an active gear is swept once by the gear, whereas

354   passive gear are likely to sweep the same area multiple times. The measured movements were

355   representative only to a certain point of what really happens: as the nets were getting too far

356   from or too close to the recording unit, it was not possible to take measurements anymore. The

357   present measurements of the movement of the leadline are therefore underestimated. However,

358   the movement of the leadline was not unlimited as the fleets were anchored on the bottom. For

359   the same reason, a major difference between longer soak durations on the estimated swept area

360   was not expected.

361   The dynamic behavior of the leadline was analysed using a simple motion metrics in the three

362   spatial dimensions, i.e., the maximum distance covered by the leadline in each dimension.

363   However, how fast the leadline moves is also expected to play a key role in the assessment of

364   the potential effects of the leadline movement on the seabed. Indeed, the fastest movements of

365   the leadline are the ones most likely to cause damage. As observed previously, marks moved

366   either regularly continuous, or with a sudden step, and speed was therefore not a good indicator.

367   Further assessment should include a spatio-temporal trajectory analysis, with focus on

368   acceleration, i.e, change in velocity with time.

369   The observations of the pilot project only covered the soaking phase of a gillnetting operation,

370   i.e., when the gear was fully deployed on the bottom, and not the retrieval of the gear, therefore

371   not covering the total potential habitat effect of bottom gillnets. Shester and Micheli (2011)

372   observed the entanglement and removal of kelp plants and gorgonian corals by set gillnets while

373   being hauled. Effects of hauling are more likely to be destructive as more power is exerted

374   through the nets (hauler) than when soaking, for which, e.g., a stone could eventually stop the

375   net. It is however known from fishermen practices that the way the gear is handled when hauling

376   can significantly reduce possible habitat damage, e.g., hauling in the current direction.

377   **Gear configuration as mitigation measure**

378   As demonstrated in this experiment, the gear configuration affects the sweeping of the nets,

379   with light nets moving significantly more than heavy ones. Whereas the general perception is

380   that heavy gears are more destructive to the habitat, such as in active gears (Kaiser *et al.*, 2002),

381   it was demonstrated here that a heavier leadline would result in less movement, being the actual

382   issue in terms of potential habitat damage of bottom-set gillnets. Therefore, gear configuration

383   has a strong mitigation effect regarding the sweeping behavior of the leadline, and habitat

384   damage could be reduced by using nets mounted with heavier leadlines.

385   In addition to the tested net configuration, i.e., light and heavy nets, other components of the

386   fishing gear in gillnets could be looked at to mitigate their habitat effects. Bridles attached to the

387   head or bottom line will give the netting different types of curves which will affect the drag

388   (Stewart and Ferro, 1985). Twine diameter, mesh size, netting hanging ratio and length of fleets,

389   as well as the way the nets are set out could also affect the drag and therefore the leadline

390   movement of bottom-set gillnets.

391   **General applicability of the results**

392   Due to the limited number of observations and choice of model, movement values presented

393   here were not meant to be predicted outside of the experimental conditions. Water flow speeds

394   during data collection were lower than the average range in coastal Danish waters (0.26 to

395   0.77m.s^{-1}) (National Geospatial-Intelligence Agency, 2013). Therefore, such experimental

396   conditions of mild sea conditions gave conservative estimates. The flow from waves, induced by

397   wind, and current, induced by both tides and wind, represents the most common flow condition

398   on the seabed for shallow water depths at our scales of interest (spatial and temporal) (Jensen

399   and Jónsson, 1987; Otto *et al.*, 1990; Myrhaug, 1995; Soulsby, 1997). The complex effects of

400   water flow, waves and wind, can change at a small scale, and influence the behavior of the gear

401   (Shimizu *et al.*, 2004). These local differences in water flow could be a reason for the significant

402   interacting effect of runs. When moving, all marks moved in a single direction in all dimensions,

403   which indicated that movements were not caused by the local action of waves, i.e., flow and

404   surge which would have resulted in, e.g., repeated forward-backward movements. When

405   moving, not all fleets moved in the same direction, which indicated that movements were not

406   caused by the overall action of waves, i.e., towards the coast. Detailed measurement of the

407   current direction and speed in further experiments could provide with a better understanding of

408   the environmental variables at stake. Very shallow waters were needed to test how to operate the

409   camera cages, and also because water was turbid at the time of data collection. Further

410   estimations should be run in deeper waters for which water flow conditions would be different,

411   as the turbulent boundary layer does not occupy the entire water column contrary to shallow

412   waters (Soulsby, 1997; Otto *et al.*, 1990). This is conditioned on an improved method that

413   allows to place an observation unit quite close to the net at such depths, e.g., using a sonar, and

414   external lightning to compensate for the reduced light conditions.

415   Because the pilot project was located in very shallow waters, a small net height was chosen. It is

416   commercial practice to work with such a net height, but higher nets may have an influence on

417   the overall gear equilibrium and drag. So may caught fish, but it is generally assumed that fish

418   would not have a great effect (Shimizu *et al.*, 2007).

419   **Supplementary material**

420   An extract of one of the video recordings is given as supplementary material at ICESJMS

421   online.

422   **Acknowledgements**

431   **References**

432   Depestele, J., Ivanović, A., Degrendele, K., Esmaeili, M., Polet, H., Roche, M., Summerbell, K.,

433   Teal, L.R., Vanelslander, B., O'Neill, F.G. 2016. Measuring and assessing the physical

434   impact of beam trawling. ICES Journal of Marine Science, 73: i15-i26.

435   E.C. 2008. Directive 2008/56/EC of the European Parliament and of the Council of 17 June

436   2008 establishing a framework for community action in the field of marine environmental

437   policy (Marine Strategy Framework Directive).

438   E.C. 2016. Community Fishing Fleet Register Data Base. Available from

439   http://ec.europa.eu/fisheries/fleet/index.cfm [Accessed on January 11th 2017].

440   Eigaard, O.R., Bastardie, F., Breen, M., Dinesen, G.E., Hintzen, N.T., Laffargue P., Mortensen,

441   L.O., Nielsen, J.R., Nilsson, H.C., O'Neill, F.G., Polet, H., Reid, D.G., Sala, A., Sköld, M.,

442   Smith, C., Sorensen, T.K., Tully, O., Zengin, M., Rijnsdorp, A.D. 2016. Estimating seabed

443   pressure from demersal trawls, seines, and dredges based on gear design and dimensions.

444   ICES Journal of Marine Science, 73: i27-i43.

445   Eno, N.C., Frid, C.L.J., Hall, K., Ramsay, K., Sharp, R.A.M., Brazier, D.P., Hearn, S., Dernie,

446   K.M., Robinson, K.A., Paramor, O.A.L., Robinson, L.A. 2013. Assessing the sensitivity of

447   habitats to fishing: from seabed maps to sensitivity maps. Journal of Fish Biology, 83: 826-

448   846.

449   EU Copernicus, 2017. Atlantic - European North West Shelf - Ocean Physics Analysis and

450   Forecast (NORTHWESTSHELF_ANALYSIS_FORECAST_PHYS_004_001_b). Available

451   from EU Copernicus Marine Service Information http://marine.copernicus.eu/services-

452   portfolio/access-to-

453   products/?option=com_csw&view=details&product_id=NORTHWESTSHELF_ANALYSIS

454   _FORECAST_PHYS_004_001_b [Accessed June 9th 2017]

455   Grabowski, J.H., Bachman, M., Demarest, C., Eayrs, S., Harris, B.P., Malkoski, V., Packer, D.,

456   Stevenson, D. 2014. Assessing the vulnerability of marine benthos to fishing gear impacts.

457   Reviews in Fisheries Science, 22: 142-155.

458   He and Pol, 2010. Fish behavior near gillnets: capture processes and influencing factors.

459   Behavior of Marine Fishes: Capture Processes and Conservation Challenges, Wiley-

460   Blackwell, pp. 183-203.

461   Hermsen, J.M., Collie, J.S., Valentine, P.C. 2003. Mobile fishing gear reduces benthic

462   megafaunal production on Georges Bank. Marine Ecology Progress Series, 260: 97-108.

463   Herrmann, B., Krag, L.A., Frandsen, Madsen, N., Lundgren, B., Stæhr, K.-J., 2009. Prediction

464   of selectivity from morphological conditions: methodology and a case study on cod (*Gadus*

465   *morhua*). Fish. Res., 97, 59-71.

466   Humborstad, O.-B., Nøttestad, L., Løkkeborg, S., Rapp, H. T. 2004. Rox-Ann bottom

467   classification system, sidescan sonar and video-sledge: spatial resolution and their use in

468   assessing trawling impacts. ICES Journal of Marine Science, 61: 53-63.

469   Jennings, S., Kaiser, M.J. 1998. The effects of fishing on marine ecosystems. Advances in

470   Marine Biology, 34: 201–212, 212e, 213–352.

471   Jensen, T.G., Jónsson, S. 1987. Measurement and analysis of currents along the Danish west

472   coast. Deutsche Hydrografische Zeitschrift, 40: 193–213.

473   Kaiser, M.J., 1998. Significance of bottom-fishing disturbance. Conservation Biology, 12:

474   1230–1235.

475   Kaiser, M.J., Spence, F.E., Hart, P.J.B., 2000. Fishing-gear restrictions and conservation of

476   benthic habitat complexity. Conservation Biology, 14: 1512-1525.

477   Kaiser, M.J., Collie, J.S., Hall, S.J., Jennings, S., Poiner, I.R. 2002. Modification of marine

478   habitats by trawling activities: prognosis and solutions. Fish and Fisheries, 3: 114-136.

479   Lucchetti, A., Sala, A. 2012. Impact and performance of Mediterranean fishing gear by side-

480   scan sonar technology. Canadian Journal of Fisheries and Aquatic Sciences, 69: 1806-1816.

481   Matuda, K. 1988. Headline height of bottom gill nets set across a water flow. Fisheries

482   Research, 6: 167–179.

483   Matuda, K. Sannomiya 1977a. Theory and design of bottom drift net. 2. Results of numerical

484   analysis on motion of gear. Bulletin of the Japanese Society of Scientific Fisheries, 43: 679–

485   687.

486   Matuda, K. Sannomiya, N. 1977b. Theory and design of bottom drift net. 1. Method of

487   numerical analysis on motion of gear. Bulletin of the Japanese Society of Scientific Fisheries,

488   43: 669–678.

489   Matuda, K. Sannomiya, N. 1978. Theory and design of bottom drift net. 3. Analytical solutions

490   of equation of motion of gear. Bulletin of the Japanese Society of Scientific Fisheries, 44: 7–

491   13.

492   Montgomerie, M., 2015. Basic fishing methods. Ed. by R. Forbes. Seafish, Edinburgh. 104 pp.

493   Myrhaug, D. 1995. Bottom friction beneath random waves. Coastal Engineering, 24: 259–273.

494   National Geospatial-Intelligence Agency of the United States Government, 2013. Sailing

495   directions for Skagerrak and Kattegat. 14th ed., 168p.

496   Neuswanger, J., Wipfli, M.S., Rosenberg, A.E., Hughes, N.F. 2016. Measuring fish and their

497   physical habitats: versatile e2D and 3D video techniques with user-friendly software.

498   Canadian Journal of Fisheries and Aquatic Sciences, 73: 1861–1873.

499   Olson, J., Clay, P.M., da Silva, P.P. 2014. Putting the seafood in sustainable food systems.

500   Marine Policy, 43: 104-111.

501   O'Neill, F.G., Summerbell, K., Breen, M. 2009. An underwater laser stripe seabed profiler to

502   measure the physical impact of towed gear components on the seabed. Fisheries Research,

503   99: 234-238.

504   Otto, L., Zimmerman, J.T.F., Furnes, G.K., Mork, M., Saetre, R., Becker, G. 1990. Review of

505   the physical oceanography of the North Sea. Netherlands Journal of Sea Research, 26: 161–

506   238.

507   R Core Team. 2016. R: A language and environment for statistical computing. R Foundation for

508   Statistical Computing, Vienna, Austria.

509   Schmidt, V.E., Rzhanov, Y. 2012. Measurement of micro-bathymetry with a GOPRO

510   underwater stereo camera pair. 2012 Oceans, IEEE, pp. 6404786.

511   Shester, G., and Micheli, F. 2011. Conservation challenges for small-scale fisheries: bycatch and

512   habitat impacts of traps and gillnets. Biological Conservation, 144: 1673-1681.

513   Shimizu, T., Takagi, T., Suzuki, K., Hiraishi, T., Yamamoto, K. 2004. Refined calculation

514   model for NaLA, a fishing net shape simulator, applicable to gill nets. Fisheries Science, 70:

515   401-411.

516   Shimizu, T., Takagi, T., Korte, H., Hiraishi, T., Yamamoto, K. 2007. Application of NaLA, a

517   fishing net configuration and loading analysis system, to bottom gill nets. Fisheries Science,

518   73: 489-499.

519   Smith, C.J., Rumohr, H., Karakassis, I., Papadopoulou, K.-N. 2003. Analysing the impact of

520   bottom trawls on sedimentary seabeds with sediment profile imagery. Journal of Expermental

521   Marine Biology and Ecology, 285-286: 479-496.

522   Soulsby, R. 1997. Dynamics of marine sands: A manual for practical applications. London:

523   Telford, 249p.

524   Stewart, P.A.M. 1988. Measurements of the effects of tidal flow on the headline heights of

525   bottom-set gillnets. Fisheries Research, 6: 181-189.

526   Stewart, P.A.M., Ferro, R.S.T. 1985. Measurements on gill nets in a flume tank. Fisheries

527   Research, 3: 29-46.

528   Struthers, D.P., Danylchuk, A.J., Wilson, A.D.M., Cooke, S.J. 2015. Action cameras: bringing

529   aquatic and fisheries research into view. Fisheries, 40: 502-512.

530   Suuronen, P., Chopin, F., Glass, C., Løkkeborg, S., Matsushita, Y., Queirolo, D., Rihan, D.

531   2012. Low impact and fuel efficient fishing - Looking beyond the horizon. Fisheries

532   Research, 119-120: 135-146.

533   Takagi, T., Shimizu, T., Korte, H. 2007. Evaluating the impact of gillnet ghost fishing using a

534   computational analysis of the geometry of fishing gear. ICES Journal of Marine Science, 64:

535   1517-1524.

536   Uhlmann, S.S., and Broadhurst, M.K. 2013. Mitigating unaccounted fishing mortality from

537   gillnets and traps. Fish and Fisheries, 16: 183-229.

538   Watson, R., Revenga, C., Kura, Y. 2006. Fishing gear associated with global marine catches. I.

539   Database development. Fisheries Research, 79: 97-102.

540   Zuur, A.F., Ieno, E.N., Elphick, C.S. 2010. A protocol for data exploration to avoid common

541   statistical problems. Methods in Ecology and Evolution, 1: 3-14.

Table 1. Specifications of individual net panels used in the experimental set-up for light and heavy gear types. Height is given as stretched height. Headline and leadline types are given as specified by the net maker Daconet (firm's internal specification without unit). Specifications differing between the two gear types, light and heavy, are emphasized in bold.

Gear specifications		Light	Heavy
Net	Type	Gillnet	
	Target species	Plaice	
Twine	Diameter	0.30 mm	
	Type	Monofil	
	Material	Nylon	
	Knot	Double	
Mesh size	Nominal (bar length)	68 mm	
Dimensions	Height (mesh depth)	1.1 m (8.5)	
	Length (knot length)	82 m (4800)	
	Hanging ratio	25%	
Headline	Type (Hau Line mono)	**1.5**	**2.5**
	Buoyancy per 100 m	**600 g**	**1200 g**
Leadline	Type (Hau sinkline lead-free)	**1.5**	**3**
	Weight per 100 m	**3.9 kg**	**11 kg**

Table 2. Run, fleet and net type for each of the eight marks on the leadline of gillnets observed in the pilot sea trial. Clip gives the total duration in min of the recorded images for each observed mark. The maximum distance (Max. distance) gives the maximum distance in m covered by the movements of each observed mark in the X, Y and Z dimensions. The maximum swept area (Max. swept area) gives the maximum swept area in m^2 covered by the movements of each observed mark in the X, Y and Z dimensions.

Mark	Run	Fleet	Net type	Clip (min)	Max. distance (m)			Max. swept area (m^2)
					X	Y	Z	
1	I	Ia	Heavy	125	0.32	0.19	0.05	0.06
2	I	Ib	Light	13	0.82	2.01	0.26	1.65
3	I	Ic	Heavy	128	0.30	0.44	0.07	0.13
4	I	Ic	Heavy	133	0.59	0.73	0.12	0.43
5	I	Ic	Heavy	101	0.21	0.56	0.06	0.12
6	II	IIa	Light	132	1.10	1.06	0.02	1.17
7	II	IIb	Heavy	29	0.14	0.29	0.04	0.04
8	II	IIb	Heavy	138	0.29	0.06	0.03	0.02

Table 3. Estimates and standard errors (se) of the parameters in the chosen model for the log expected maximum movement of the leadline. All parameters were tested significant at p-value <0.001.

Parameters	Estimate (se)
β *(Dimension$_i$)*	
Dimension X	-5.56 (0.54)
Dimension Y	-5.43 (0.54)
Dimension Z	-7.42 (0.54)
γ *(Net$_i$, Run$_i$)*	
Light net, Run I	3.29 (0.69)
Light net, Run II	0 (0)
Heavy net, Run I	-0.19 (0.54)
Heavy net, Run II	-0.34 (0.59)

Fig. 1. The observation unit.
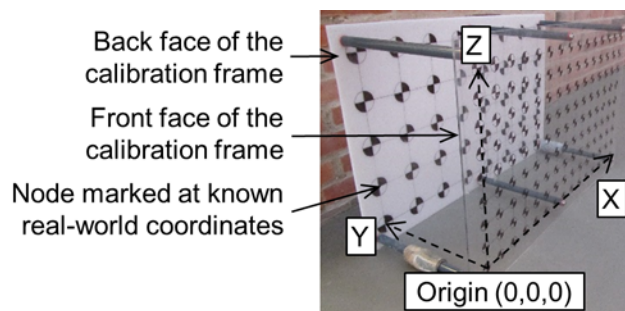
Fig. 2. The calibration frame.
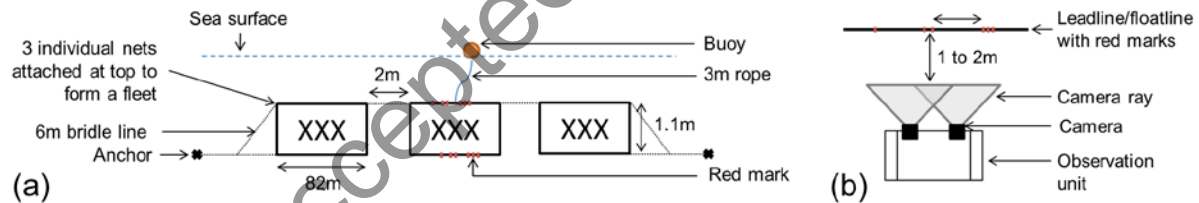
Fig. 3. Experimental set-up for stereo imaging with (a) side view of a fleet, i.e., a ganged sequence of 3 individual gillnets, set on the bottom, (b) top view of the observation unit positioned in front of a net.
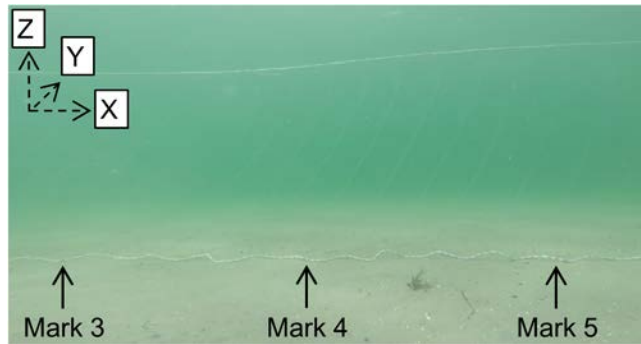
Fig. 4. An in situ example (fleet Ic) of the positions of three different marks (identified from 3 to 5) on the leadline of the same net recorded in the three dimensions (X, Y and Z).
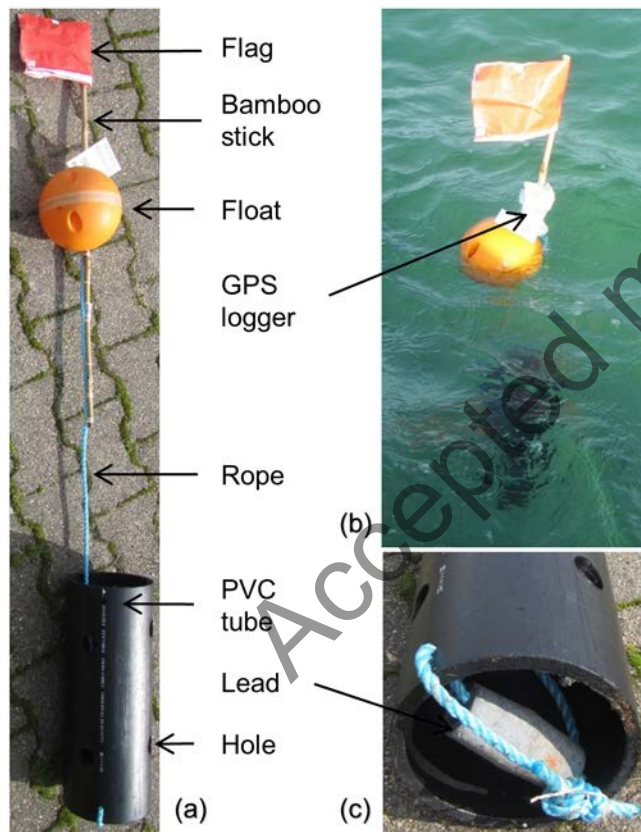

Fig. 5. Drifting device to measure current speed and direction with (a) full view of the device, (b) view of the device at sea, and (c) close-up view of the lower end of the PVC tube which allows to measure at the median net height in the water column. Two similar devices were left drifting between the nets during data collection.
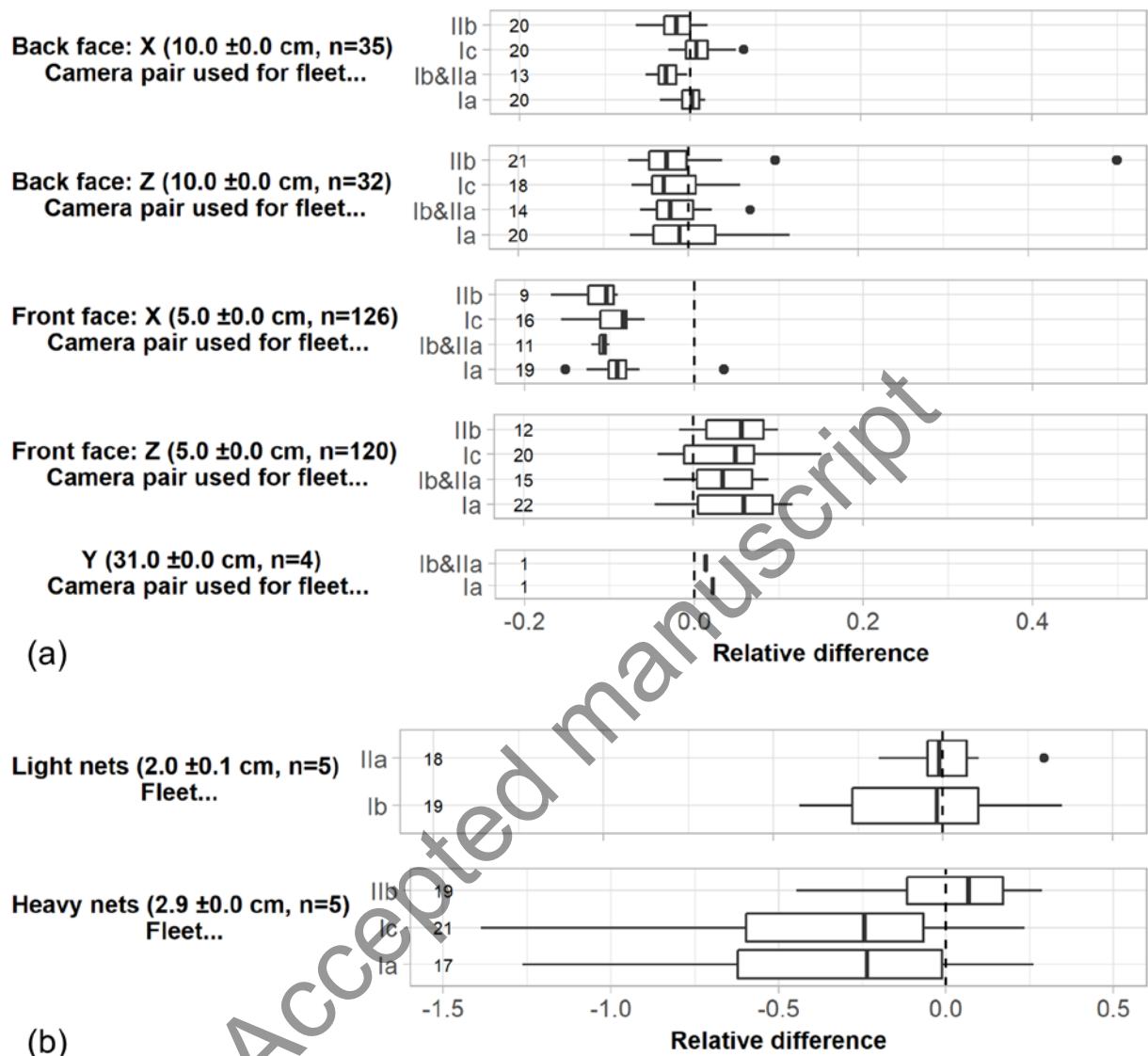
Fig. 6. (a) Relative difference of the calculated distances (with Vidsync) compared to the

measured distances (with a measuring tape) between two nodes of the calibration frame on the

back and front faces in the X (horizontal) and Z (vertical) dimensions, and between the back and

front faces of the calibration frame (Y). (b) Relative difference of the calculated distances (with

Vidsync) compared to the measured distances (with a measuring tape) between two coloured

threads on the leadline of light and heavy bottom gillnets. On both (a) and (b), the horizontal

dashed line stands for reference as no difference between measured and calculated. The distances measured are given as an average ±standard deviation with n the number of observations on the left of each plot. The number of the calculated distances used for the comparison is given on the right of each corresponding boxplot.
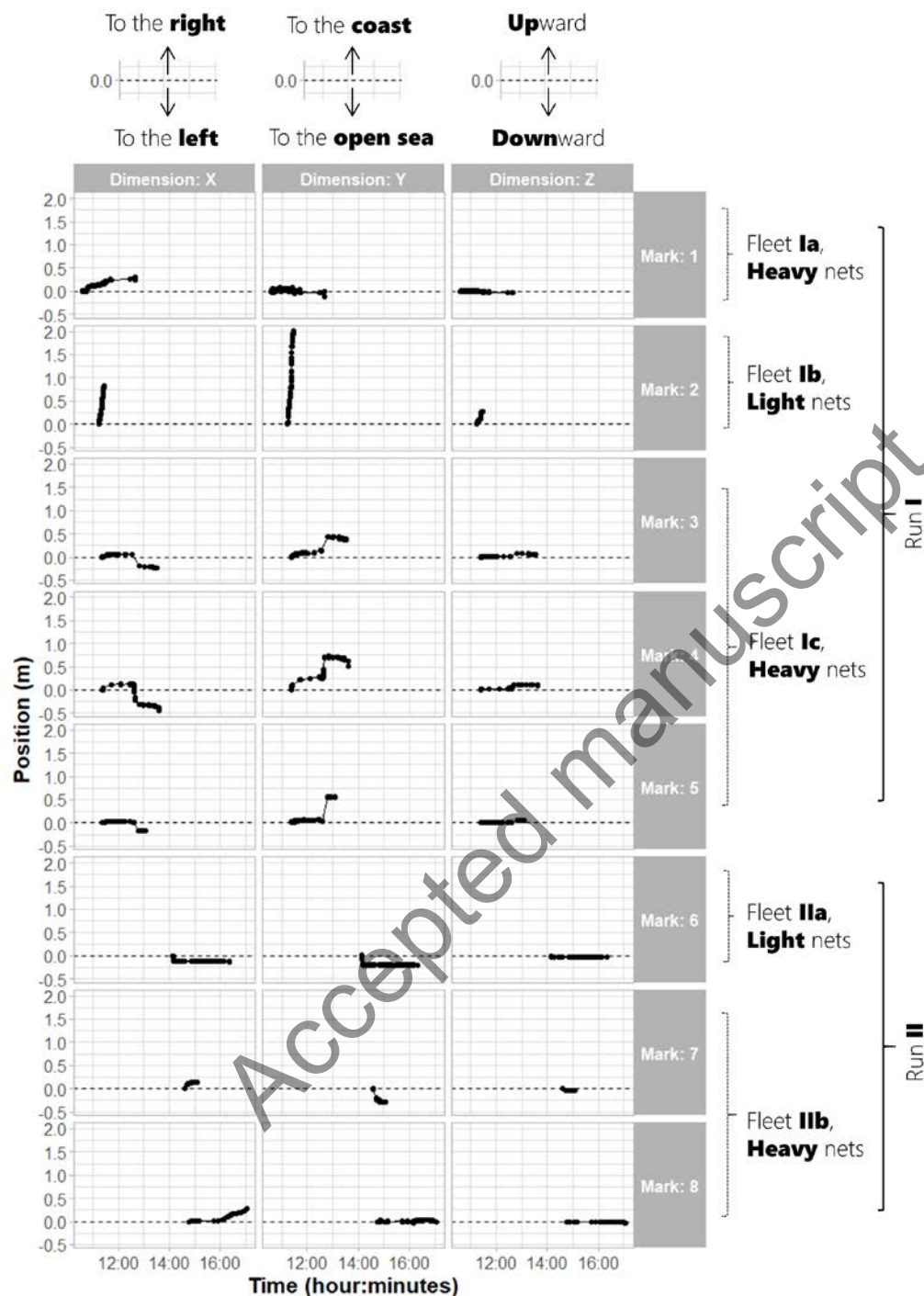
Fig. 7. Time plot of the relative position of the eight marks on the leadline of light and heavy gillnets observed in the pilot sea trial, in the X, Y and Z dimensions. The relative position is given in m as the distance from the initial position (horizontal dashed line). Time is given as the real time of the day in hour:minutes.
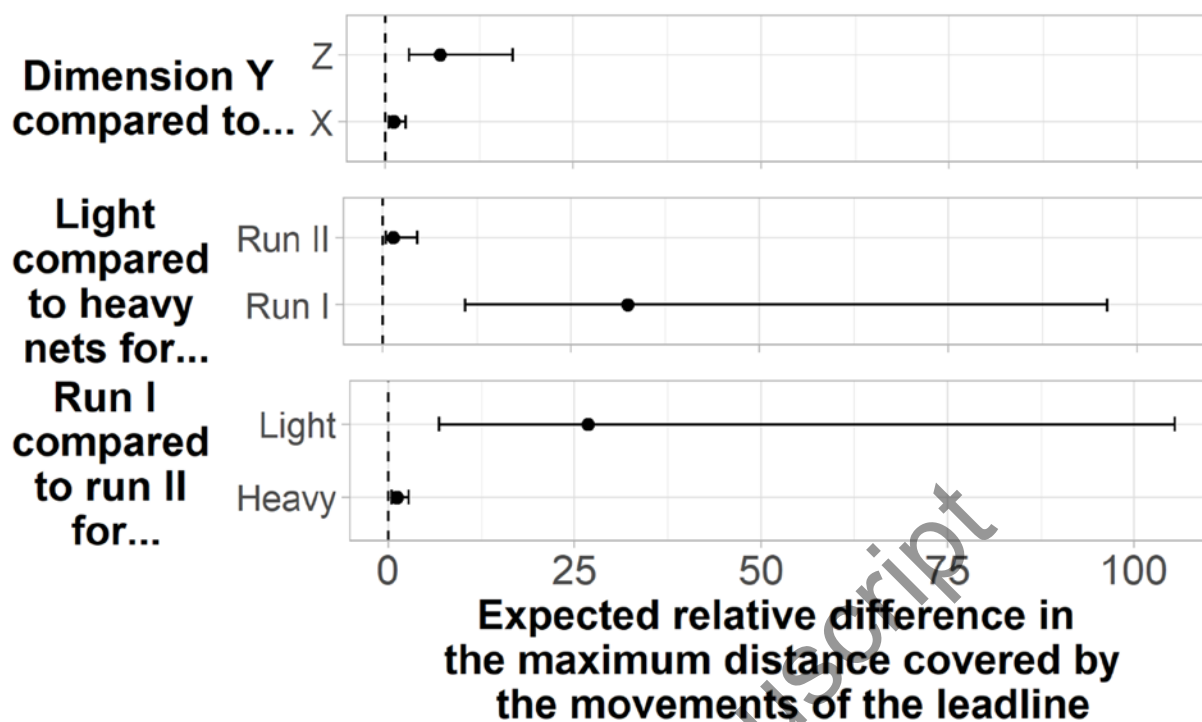
Fig. 8. Expected relative difference (95% confidence limits) in the maximum distance covered by the movements of the leadline for the different experimental configurations.